Design of hybrid MoS2/photonic devices compatible with technological constraints

Jean-Baptiste Dory, Olivier Gauthier-Lafaye, Pascal Dubreuil, Inès Massiot, Stéphane Calvez, Adnen Mlayah

Design of hybrid MoS_2/photonic devices compatible with technological constraints

Design of hybrid MoS_2/photonic devices compatible with technological constraints

Jean-Baptiste Dory[1,2], Olivier Gauthier-Lafaye[2], Pascal Dubreuil[2], Inès Massiot[2], Stéphane Calvez[2], Adnen Mlayah[1,2]

1. CEMES-CNRS, Université de Toulouse, Toulouse, France

2. LAAS-CNRS, Université de Toulouse, Toulouse, France

Corresponding authors : amlayah@laas.fr, olivier.gauthier-lafaye@laas.fr

Abstract

The integration of transition metal dichalcogenide layers into photonic devices is a current challenge in the field of 2D materials. Based on numerical simulations, this work explores the design of devices combining an MoS_2 monolayer with planar photonic gratings sustaining localized optical resonances. A special attention is paid to the technological constraints. The optical response of six devices is compared taking into account the limitations imposed by the growth conditions of the MoS_2 layer and the processing of the resonant optical gratings. The reported photonic devices composed of grating filters and a backside reflector on silicon and silica substrates exhibit a theoretical absorption by the MoS_2 layer between 85 and 99% at 532 nm. The numerical simulations further show that the addition of an Al_2O_3 encapsulation layer to protect the MoS_2 monolayer results in an increase of the performance of the devices. These hybrid MoS_2 based photonic devices are promising technological platforms for the study of the optical properties of integrated MoS_2 monolayers.

1. Introduction

Transition Metal Dichalcogenides (TMD) are two-dimensional (2D) semiconductor materials with astonishing physical properties [1] thanks to their stunning excitonic binding energy and valley spin properties [2]. Numerous works reported numerical simulations of devices achieving near perfect absorption by stacking these ultrathin dichalcogenide layers on or under metallic layers and antenna [3-12]. The devices with plasmonic structures on top of a TMD monolayer present the advantage of concentrating the electromagnetic field in the 2D material [13] paving the way for systems exploiting enhanced photoluminescence (PL) emission and/or photocurrent (PC) conversion. Thus, some works report measurements of significant PL enhancement of TMD monolayers in hybrid photonic devices with various metallic 2D structures near the TMD material [14-22]. However, the contact between the metal and the TMD material could be responsible for a quenching of TMD emission due to charge transfer [23-25]. To avoid this detrimental effect while keeping the ability to demonstrate exceptional absorption [26], the use of less common metals as Gallium [27], or stacked spacing layers [28] or only dielectric materials [29] have been reported.

A general review of the reported experimental demonstrations involving TMDs shows that the transition from isolated lab-scale objects to large-scale integrated devices comes with a significant degradation of the TMD material performances [30]. Given the recent demonstration of the synthesis of high-quality TMD monolayers on a wafer scale [31], one of the key challenges remaining to make TMD-based devices a reality is to develop integration methods compatible with TMD materials [1, 32]. Integration of TMD materials can be significantly improved by taking into account the technological and experimental constraints into the design of devices. As TMD materials show limited stability when exposed to air [33], an encapsulation layer is mandatory to protect the TMD material from contact with the atmosphere [34-38] or from detrimental subsequent technological steps. Similarly, should the

TMD material be deposited by CVD methods, the underlying multi-layer coated substrate has to withstand the high deposition temperature (above 400°C).

In this work, we investigate hybrid devices with a MoS_2 monolayer incorporated into grating based photonic cavities. The devices are designed to achieve a maximum optical absorption by the MoS_2 layer at a target excitation wavelength (532 nm in our case). The MoS_2 monolayer is integrated between a reflector and a resonant grating. The several stacks are conceived to protect the MoS_2 materials from degradation induced by the most reactive integration steps, in particular etching processes. Two types of resonant gratings are compared: an infinitely long grating-mode resonant filter (GMRF) and a more realistic cavity resonator integrated grating filter (CRIGF) with finite lateral dimensions. A CRIGF is composed of a grating coupler (GC) between two distributed Bragg reflectors (DBRs) on top of a waveguide layer [39]. Under optical illumination of the GC, a fraction of the incoming light is injected into a single-mode confined in the lateral cavity formed by the two DBRs. As demonstrated in [40], a CRIGF can be viewed as a small foot-print, folded GMRF device. Its small footprint is particularly interesting in the case of ultrathin 2D materials of which lateral size may be too small to allow an efficient coupling with a GMRF device. In this work, the MoS_2 monolayer is incorporated just below this waveguide resonator (Figure 1) leading to the absorption of the resonating optical mode by the MoS_2.

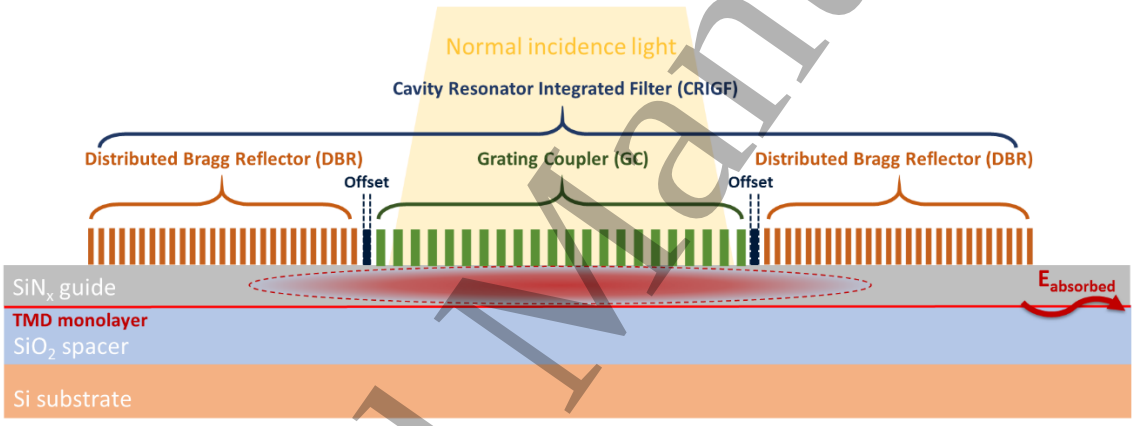

Figure 1: Schematic of the hybrid MoS_2/photonic vertical stack with description of CRIGF grating parts. The device is designed to focus the incident light in the SiN_x guiding layer. This configuration maximizes the absorption by the TMD monolayer directly below this guiding layer.

2. Numerical tools

Hybrid devices made of photonic structures and 2D materials combine micro and nanoscale engineering which, for modelling, implies microscopic meshing with locally sub-nanoscale precision. To maintain a reasonable calculation time, numerical simulations were performed using 2D-FMM methods [41] with an S-matrix algorithm [42]. The calculations are carried out using up to 1200 Fourier components for stacks with an entire CRIGF structure. For the CRIGF-based devices, the incoming light is under normal incidence with transverse electric (TE) polarisation; its intensity is Gaussian-shaped and overlaps only with the central part of the grating coupler. For GMRF-based devices, the calculations were performed for a plane wave at normal incidence, in TE polarization. The complex refractive index of the materials used in the simulations are provided in the Supplementary Information section. Absorption of the here considered dielectric materials (SiO_2, SiN_x and Al_2O_3) is negligible in the wavelength range of interest (500 to 800 nm). Thus, absorption occurs only within the MoS_2 layer and the Si substrate or back side reflector.

3. Discussion

3.1. Optimal numerical solutions

For each investigated device, the geometrical parameters of the stack were optimized to maximize the absorbed fraction of the incident light. Table 1 summarizes these parameters and the calculated optical absorption by the MoS_2 layer integrated in the GMRF and CRIGF structures compared to a reference made of a MoS_2 layer on 90 nm SiO_2/Si substrate (hereafter named $MoS_2/SiO_2/Si$).

Table 1 : Synthesis of geometrical parameters and calculated absorption performance of six studied devices compare to the theoretical optical response of MoS_2 monolayer on 90nm SiO_2/Si substrate.

Grating type	SiN_x grating				SiN_x guide	Al_2O_3 encapsulation	**Absorption at 532nm (%)**	SiO_2 spacer	Mirror	
	Thickness (nm)	Period (nm)	Filling factor	Offset factor	Thickness (nm)	Thickness (nm)		Thickness (nm)	Material	T_f (°C)
$MoS_2/SiO_2/Si$	- - -	- - -	- - -	- - -	- - -	- - -	**20.9**	90	Si bulk	1414
GMRF on Ag	135	294	0.50	- - -	125	- - -	**99.1**	250	Silver	961
GMRF on Al	110	292	0.50	- - -	130	- - -	**97.6**	225	Aluminium	660
GMRF on Si	120	298	0.50	- - -	110	- - -	**85.8**	250	Si bulk	1414
CRIGF on Si	120	298	0.50	1.00	110	- - -	**82.0**	250	Si bulk	1414
CRIGF with encapsulation	120	312	0.70	1.10	60	10	**84.9**	285	Si bulk	1414
Reversed CRIGF	60	288	0.45	1.05	120	20	**89.1**	210	Aluminium	660

Figure 2.a shows the investigated device consisting of a SiN_x GMRF structure with a planar guiding layer on a monolayer MoS_2 onto a silicon oxide film with a backside metallic mirror forming a vertical cavity. Optimisation of the layer thicknesses and GMRF parameters (see Table 1) led to the selection of a particular structure that allows the absorption of 99.1% of the incident light at 532 nm in the MoS_2 monolayer as shown in Figure 2.c.

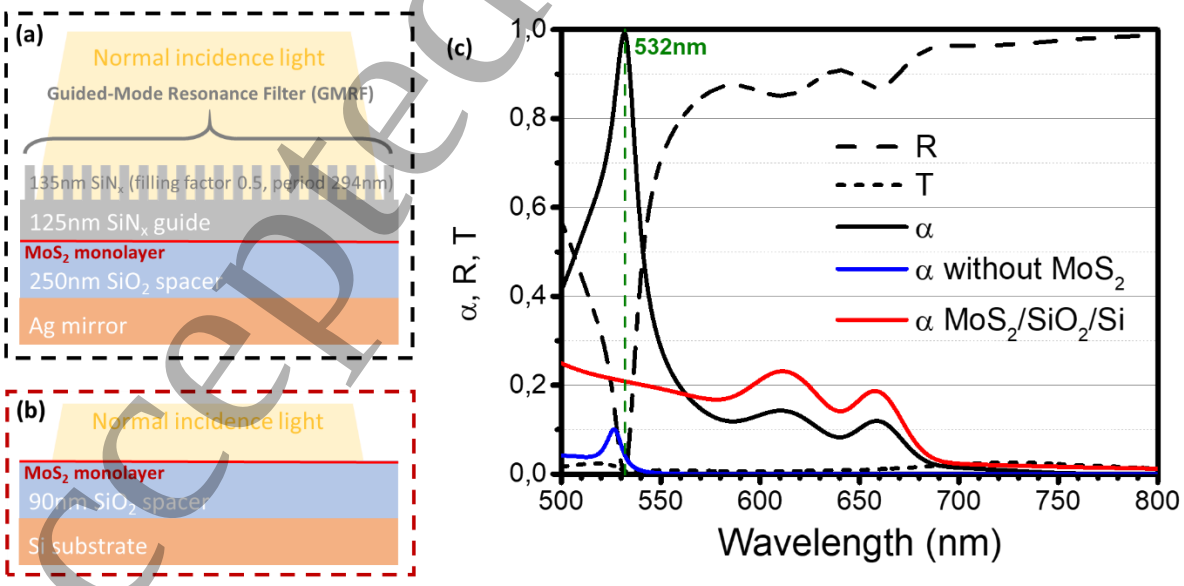

Figure 2: Schematics of GMRF/MoS_2 with Ag reflector vertical stacks (a), schematics of $MoS_2/SiO_2/Si$ stack (b) and calculated optical response spectra of three devices (c): reflection, transmission and absorption fraction of energy calculated

for GMRF/MoS_2 with Ag reflector device (black curves), absorption of the latter device without MoS_2 layer (blue curve) and absorption of standard MoS_2/SiO_2/Si stack (red curve).

The near-perfect absorption at 532 nm is obtained owing to the coupling of the resonance of the GMRF structure with the B and C-exciton resonances of the MoS_2 layer. Indeed, the A and B exciton absorption bands are clearly visible around 660 and 610 nm, respectively; whereas the one of the C-exciton arises below 500nm [14, 43]. The absorption of the same device but without its MoS_2 layer is significantly lower. This residual absorption arises from the enhancement of the electromagnetic field near the GMRF structure and the absorption of the SiN_x layer. Comparison of the GMRF/Ag reflector device with and without the MoS_2 layer shows that the MoS_2 layer absorbs the main part of the incident light (see the Supplementary Information). Since the experimental properties of MoS_2 are generally studied for flakes reported or grown on a 90nm SiO_2/Si substrate (see Figure 2.b), we calculate that 20.9% of the incident light is absorbed in this reference stack at 532 nm, a value consistent with the results reported in the literature [44]. The GMRF with Ag reflector enhances the optical absorption by the MoS_2 layer by a factor 5 compared to the MoS_2/SiO_2/Si reference.

The GMRF-based structure on Ag reflector shows impressive performances, however its fabrication faces several technological challenges. Firstly, SiN_x film is commonly grown using plasma assisted processes under reactive conditions (nitride atmosphere and/or nitride precursors) which may create defects in the atomic structure of the TMD layer during the early stages of the deposition. Secondly, silver (back reflector) is rarely used in microelectronic devices, because of its low thermal stability incompatible with the MoS_2 deposition temperature. The melting temperature of the material used as back reflector is given in the Table 1 as an indication of its thermal stability. One must keep in mind that degradation of the reflector (delamination, phase segregation,…) occurs at temperatures way below its melting temperature. The incompatibility between the low thermal stability of silver and the MoS_2 deposition temperature can only be solved using a transfer of the MoS_2 layer or by deposition of the Ag layer, after the growth of the MoS_2 layer, combined with a challenging back side thinning down to the spacer layer. Vertical DBRs based on dielectric materials are a potential substitute to metallic reflector. However, their fabrication requires an excellent repeatability (in composition and thickness) of dielectric deposition steps and the multiplicity of layers which can be a source of stack delamination.

To bypass these technological issues, alternative structures need to be explored and compared to the GMRF based near-perfect absorber structure. Furthermore, the sharp resonance generated in the hybrid photonic device is well adapted to the illumination by spectrally coherent light sources, which can be focused to the active region of the device. To this aim, CRIGF structures, consisting of a resonant grating of finite length and an additional lateral optical confinement have been shown to facilitate high-Q cavity operation under focused laser spot [45]. As such, CRIGFs are also more amenable to lead to high performance devices with a spatially-restricted uniformity.

3.2. Alternative devices based on practical integration considerations

In this work, the GC of the CRIGF structures is composed of 41 periods matching a beam width of about 12 µm. As the period of the DBRs is half the GC period, considering DBRs composed of 100 periods, the total width of the device is 45 µm at maximum. Figure 3.a shows the theoretical optical response of three types of hybrid CRIGF/MoS_2 devices.

The first CRIGF/MoS_2-based design is similar to the previously studied GMRF/MoS_2 design (see Figure 2.a) with the GMRF structure and Ag mirror replaced respectively by a CRIGF structure and a Si substrate (see Figure 3.b). As reported in Table 1, the Ag mirror improves significantly the absorption by the MoS_2 layer compared to the same device on a standard silicon substrate (99.1 compared to

85.8%). However, the stack on Si substrate is compatible with the direct deposition of TMD materials at high temperature (around 650°C). With the CRIGF structure, the absorption by the TMD layer is weaker than with a GMRF structure (82.0 instead of 85.8%). This is due to the finite lateral size of the CRIGF. Indeed, for a GMRF limited to 41 periods (as the GC part of the CRIGF) and using an illumination source with the same gaussian beam waist, the theoretical absorption by the MoS_2 layer in the GMRF decreases to 80.8% (as compared to the initial 85.8%). Thus, when considering realistic lateral dimensions of the GMRF structure, better performances are predicted for the CRIGF structure compared to the GMRF.

The second CRIGF design (see Figure 3.c) is composed of an additional alumina Al_2O_3 layer intercalated between the MoS_2 monolayer layer and the SiN_x guide. The Al_2O_3 layer is a protective capping layer which could be deposited to prevent contamination and degradation of the MoS_2 layer during the reactive processes. Indeed, Al_2O_3 is airtight and has a good chemical stability. In addition, Al_2O_3 is commonly obtained by atomic layer deposition (ALD), a softer process compared to chemical or physical vapour deposition (CVD or PVD). With a 10 nm thick Al_2O_3 layer and optimized parameters of the CRIGF (see values in Table 1), the maximum of absorption by the MoS_2 layer reaches 84.9% due to a better confinement of the optical mode at 532 nm. Hence, the protective Al_2O_3 integrated in the CRIGF/MoS_2 device is beneficial as it increases the achievable maximum of absorption by the MoS_2 layer.

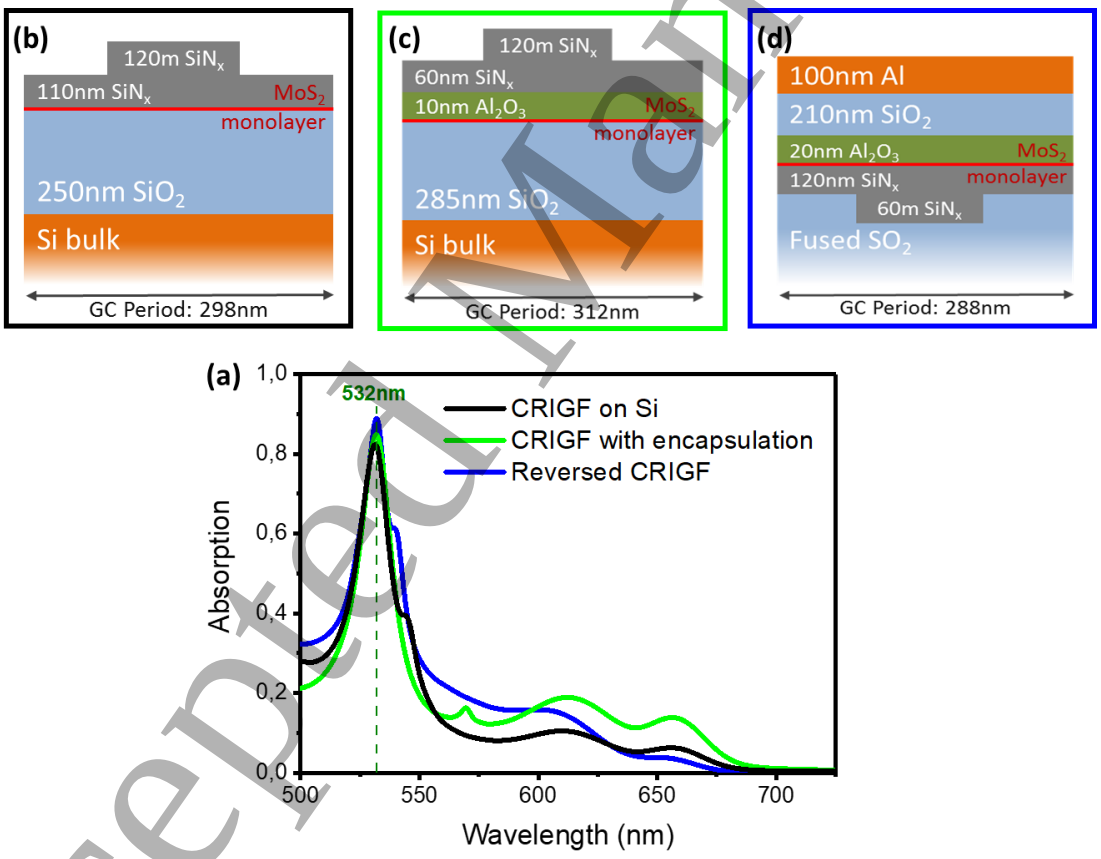

Figure 3: Schematics of the vertical stack and calculated optical response spectra of three hybrid CRIGF/MoS_2 structures: CRIGF on Si (b, black), CRIGF with encapsulation (c, green) and reversed CRIGF (d, blue).

Finally, a third CRIGF-based design is considered (Figure 3.d). It involves an inverted fabrication process flow allowing the integration of a metal mirror after the growth of the MoS_2 layer. In this way, the metal is kept below its melting temperature which can be close to the MoS_2 growth temperature (650°C) in the case of Aluminium for example. This reversed design is based on a transparent fused

silica substrate which permits a back side optical excitation. After partial etching of the substrate to fabricate the CRIGF structure, the corrugated substrate is covered by SiN_x. The MoS_2 layer would then be grown onto the SiN_x and almost no change in the nucleation and growth of the 2D material are expected compared to SiO_2 substrate as both dielectrics are amorphous materials. Because of the inversion in the integration steps, the protective Al_2O_3 layer is incorporated between the MoS_2 layer and the SiO_2 spacer. In this reversed CRIGF-based design, the encapsulation of the MoS_2 layer is essential as the oxidizing conditions under which the SiO_2 is deposited may damage the MoS_2 and introduce defects that strongly alter its optical absorption and emission properties. Finally, an aluminium reflector is added on the top of the device. Despite its slightly lower reflectance at 532 nm, Aluminium is preferred to silver due to its better thermal stability (see Table 1). According to the calculations with the reversed CRIGF-based design, the optical absorption by the MoS_2 layer reaches 89.1% at 532 nm. The integration of emerging 2D compounds in 3D devices is challenging considering the potential detrimental impact of the integration processes on the performances of the TMD materials [30]. The latter device anticipates several potential technological fabrication limitations while exhibiting impressive absorption as compared to the other CRIGF devices investigated in this work.

4. Conclusion

In summary, using numerical simulations, we found that the integration of a 2D MoS_2 layer between a CRIGF or GMRF structure and a reflector enhances the optical absorption by the MoS_2 layer to 85 to 99% as compared to the ≈20% achieved with the standard MoS_2/90 nm SiO_2/Si stack. The increase is mainly due to the coupling of the resonance sustained by the CRIGF or the GMRF with the MoS_2 excitonic absorption. The calculated absorption by the MoS_2 layer implemented in the CRIGF-based device is higher than the one reached with the GMRF-based device. Furthermore, the substitution of the Si substrate by an aluminium back reflector and the addition of a capping layer increase the theoretical absorption by the MoS_2. The designed devices are compatible with the material thermal and chemical constraints and technological processes and their optical response is suitable for studying the optical properties of integrated MoS_2 monolayers. This investigation of hybrid TMD/photonic devices is a contribution to the understanding of the impact of integration processes on TMD materials, identified as the main current challenge preventing an ubiquitous use of 2D TMD materials [1, 30].

5. References

[1] Stanford M G, Rack P D and Jariwala D 2018 Emerging nanofabrication and quantum confinement techniques for 2D materials beyond graphene *2D Mat. Appl.* **2** 20

[2] Wang G, Marie X, Gerber I, Amand T, Lagarde D, Bouet L, Vidal M, Balocchi A, and Urbaszek B 2015 Giant Enhancement of the Optical Second-Harmonic Emission of WSe_2 Monolayers by Laser Excitation at Exciton Resonances *Phys. Rev. Lett*. **114** 097403

[3] Jariwala D, Davoyan A R, Tagliabue G, Sherrott M C, Wong J and Atwater H A 2018 Near-unity absorption in van der Waals semiconductors for ultrathin optoelectronics *Nano Lett.* **16** 5482-5487

[4] Li H, Qin M, Wang L, Zhai X, Ren R and Hu J 2017 Total absorption of light in monolayer transition-metal dichalcogenides by critical coupling *Opt. Express* **25**, 31614

[5] Li H-J, Ren Y-Z, Hu J-G, Qin M and Wang L-L 2018 Wavelength-selective wide-angle light absorption enhancement in monolayers of transition-metal dichalcogenides J. *Lightwave Technol.* **36**, 16

[6] Nong J, Da H, Fang Q, Yu Y and Yan X 2018 Perfect absorption in transition metal dichalcogenides-based dielectric grating *J. Phys. D : Appl. Phys.* **51**, 375105

[7] Jiang X, Wang T, Xiao S, Yan X, Cheng L and Zhong Q 2018 Approaching perfect absorption of monolayer molybdenum disulfide at visible wavelengths using critical coupling *Nanotechnol.* **29**, 335205

[8] Zhou P, Zheng G G, Chen Y Y, Xian F L and Xu L H 2018 Spectral-selective high-efficient light absorption of large-area monolayer transition-metal dichalcogenides via critical coupling *Superlattices Microstruct.* **120**, 436-440

[9] Bahauddin S M, Robatjazi H and Thomann I 2016 Broadband absorption engineering to enhance light absorption in monolayer MoS_2 *ACS. Photonics* **3**, 853-862

[10] Cao J, Yang G, Wang J, Gao S, Lu Y, Sun R and Yan P 2017 Enhanced optical absorption of monolayer WS2 using Ag nanograting and distributed Bragg reflector structures *Superlattices Microstruct.* **112**, 218-223

[11] Li J, Chen X, Yi Z, Yang H, Tang Y, Yi Y, Yao W, Wang J and Yi Y 2020 Broadband solar energy absorber based on monolayer molybdenum disulfide using tungsten elliptical arrays *Mat. Today Energy* **16**, 100390

[12] Li J, Chen Z, Yang H, Yi Z, Chen X, Yao W, Duan T, Wu P, Li G and Yi Y 2020 Tunable broadband solar energy absorber based on monolayer transition metal dichalcogenides materials using Au nanocubes *Nanomat.* **10**, 257

[13] Barghouti M E, Akjouj A and Mir A 2018 Effect of MoS_2 layer on the LSPR in periodic nanostructures *Optik* **171**, 237-246

[14] Najmaei S, Mlayah A, Arbouet A, Girard C, Léotin J and Lou J 2014 Plasmonic pumping of excitonic photoluminescence in hybrid MoS_2 Au nanostructures *ACS Nano* **8**, 12682-12689

[15] Sobhani A, Lauchner A, Najmaei S, Ayala-Orozco C, Wen F, Lou J and Halas N J 2014 Enhancing the photocurrent and photoluminescence of single crystal monolayer MoS_2 with resonant plasmonic nanoshells *Appl. Phys. Lett.* **104**, 031112

[16] Butun S, Tongay S and Aydin K 2015 Enhanced light emission from large-area monolayer MoS_2 using plasmonic nanodisc Arrays *Nano. Lett.* **15**, 2700-2704

[17] Lee B, Park J, Han H, Ee H-S, Naylor C H, Liu W, Johnson A T C and Agarwal R 2015 Fano resonance and spectrally modified photoluminescence enhancement in monolayer MoS_2 Integrated with plasmonic nanoantenna array *Nano Lett.* **15**, 3646-3653

[18] Li J, Ji Q, Chu S, Zhang Y, Li Y, Gong Q, Liu K and Shi K 2016 Tuning the photo-response in monolayer MoS_2 by plasmonic nano-antenna *Sci. Rep.* **6**, 23626

[19] Wang Z, Dong Z, Gu Y, Chang Y-H, Zhang L, Li L-J, Zhao W, Eda G, Zhang W, Grinblat G, Maier S A, Yang J K W, Q C-W and Wee A T S 2016 Giant photoluminescence enhancement in tungsten-diselenide–gold plasmonic hybrid structures *Nat. Comm.* **7** 11283

[20] Mukherjee B, Kaushik N, Tripathi R P N, Joseph A M, Mohapatra P K, Dhar S, Singh B P, Pavan Kumar G V, Simsek E and Lodha S 2017 Exciton Emission intensity modulation of monolayer MoS_2 via Au plasmon coupling *Sci. Rep.* **7**, 41175

[21] Ni P, De Luna Bugullo A, Arellano Arreola V M, Flores Salazar M, Strupiechonski E, Brändli V, Sawant R, Alloing B and Genevet P 2019 Gate-Tunable Emission of exciton–plasmon polaritons in hybrid MoS_2-gap-mode metasurfaces *ACS Photonics* **6**, 1594-1601

[22] Song J, Kwon S, Kim E, Kim B, Kim D-W, Lee S-Y and Yee K-J 2020 Enhanced photoluminescence of MoS_2-Au nanostructures: nanotriangle and nanohole arrays *Current Appl. Phys.* **20**, 703-706

[23] Bhanu U, Islam M R, Tetard L and Khondaker S I 2014 Photoluminescence quenching in gold - MoS_2 hybrid nanoflakes *Sci. Rep.* **4** 5575

[24] Zhang L, Yan H, Sun X, Dong M, Yildirim T, Wang B, Wen B, Neupane G P, Sharma A, Zhu Y, Zhang J, Liang K, Liu B, Nguyen H T, Macdonald D and Lu Y 2019 Modulated interlayer charge transfer dynamics in a monolayer TMD/metal junction *Nanoscale* **11** 418-425

[25] Abid I, Benzo P, Jia S, Zhang J, Yuan J, Dory J-B, Gauthier Lafaye O, Péchou R, Mlayah A and Lou J 2021 Plasmon damping and charge transfer pathways in Au@$MoSe_2$ nanostructures *Mat. Todays Nano* **15** 100131

[26] Feng Y, Wu Q Y S, Wang B, Fan Y and Liu Y 2020 Design of narrowband perfect absorber for enhancing photoluminescence in atomically thin WSe_2 *Opt. Comm.* **454**, 124443

[27] Catalan-Gomez S, Garg S, Redondo-Cubero A, Gordillo N, de Andrés A, Nucciarelli F, Kim S, Kung P and Pau J L 2019 Photoluminescence enhancement of monolayer MoS_2 using plasmonic gallium nanoparticles *Nanoscale Adv.* **1**, 884

[28] Han C and Ye J 2020 Polarized resonant emission of monolayer WS_2 coupled with plasmonic sawtooth nanoslit array *Nat. Comm.* **11**, 713

[29] Bucher T, Vaskin A, Mupparapu R, Löchner F J F, George A, Chong K E, Fasold S, Neumann C, Choi D-Y, Eilenberger F, Setzpfandt F, Kivshar Y S, Pertsch T, Turchanin A and Staude I 2019 Tailoring photoluminescence from MoS_2 monolayers by mie-resonant metasurfaces *ACS Photon.* **6**, 1002-1009

[30] Lanza M, Smets Q, Huyghebaert C and Li L-J 2020 Yield, variability, reliability, and stability of two-dimensional materials based solid-state electronic devices *Nat. Comm.* **11** 5689

[31] Yu H, Liao M, Zhao W, Liu G, Zhou X J, Wei Z, Xu X, Liu K, Hu Z, Deng K, Zhou S, Shi J-A, Gu L, Shen C, Zhang T, Du L, Xie L, Zhu J, Chen W, Yang R, Shi D and Zhang G 2017 Wafer-Scale Growth and Transfer of Highly-Oriented Monolayer MoS_2 Continuous Films *ACS Nano* **11** 12001−12007

[32] Emmanuele R P A, Sich M, Kyriienko O, Shahnazaryan V, Withers F, Catanzaro A, Walker P M, Benimetskiy F A, Skolnick M S, Tartakovskii A I, Shelykh I A and Krizhanovskii D N 2020 Highly nonlinear trion-polaritons in a monolayer semiconductor *Nat. Comm.* **11** 3589

[33] Gao J, Li B, Tan J, Chow P, Lu T-M and Koratkar N 2016 Aging of transition metal dichalcogenide monolayers *ACS Nano* **10**, 2628−2635

[34] Ahn S, Kim G, Nayak P K, Yoon S I, Lim H, Shin H-J and Shin H S 2016 Prevention of transition metal dichalcogenide photodegradation by encapsulation with h-BN layers *ACS Nano* **10**, 8973−8979

[35] Mahyavanshi R D, Kalita G, Singh R, Kondo M, Dewa T, Kawahara T, Umero M and Tanemura M 2017 Encapsulation of transition metal dichalcogenides crystals with room temperature plasma deposited carbonaceous films *RSC Adv.* **7**, 41136

[36] Xu X, Chen Z, Sun B, Zhao Y, Tao L and Xu J-B *2019* Efficient passivation of monolayer MoS_2 by epitaxially grown 2D organic crystals *Sci. Bulletin* **64**, 1700–1706

[37] Lee K-N, Bang S, Duong N T, Yun S J, Park D Y, Lee J, Choi Y C and Jeong M S *2019* Encapsulation of a monolayer WSe_2 phototransistor with hydrothermally grown ZnO nanorods *ACS Appl. Mater. Interfaces* **11**, 20257−20264

[38] Canton-Vitoria R, Sayed-Ahmad-Baraza Y, Humbert B, Arenal R, Ewels C P and Tagmatarchis N 2020 Pyrene coating transition metal disulfides as protection from photooxidation and environmental aging *Nanomat.* **10**, 363

[39] Kintaka Majima K T, Inoue J, Hatanaka K, Nishii J and Ura S 2012 Cavity-resonator-integrated guided-mode resonance filter for aperture miniaturization *Opt. Express*. **20** 1444-1449

[40] Rassem N, Fehrembach A-L and Popov E 2015 Waveguide mode in the box with an extraordinary flat dispersion curve *J. Opt. Soc. Am. A* **32** 420

[41] Moharam M G, Gaylord T K, Grann E B and Pommet D A 1995 Formulation for stable and efficient implementation of the rigorous coupled-wave analysis of binary gratings *JOSA A* **12** 1068–1076

[42] Li L 1996 Formulation and comparison of two recursive matrix algorithms for modeling layered diffraction gratings *J. Opt. Soc. Am. A* **13** 1024

[43] Korn T, Heydrich S, Hirmer M, Schmutzler J and Schüller C 2011 Low-temperature photocarrier dynamics in monolayer MoS_2 *Appl. Phys. Lett.* **99**, 102109

[44] Janisch C, Song H, Zhou C, Lin Z, Elias A L, Ji D, Terrones M, Gan Q and Liu Z 2016 MoS_2 monolayers on nanocavities: enhancement in light-matter interaction *2D Mat.* **3** 025017

[45] Buet X, Daran E, Belharet D, Lozes-Dupuy F, Monmayrant A and Gauthier-Lafaye O 2012 High angular tolerance and reflectivity with narrow bandwidth cavity-resonator-integrated guided-mode resonance filter *Opt. express* **20** 9322–9327